Surface state and resonance effects in electron-pair emission from Cu(111)

F. O. Schumann,* R. S. Dhaka, G. A. van Riessen,† Z. Wei, and J. Kirschner
Max-Planck-Institut für Mikrostrukturphysik, Weinberg 2, DE-06120 Halle, Germany
(Received 18 May 2011; revised manuscript received 28 July 2011; published 6 September 2011)

We report on an electron-pair emission study from a Cu(111) surface excited by electron impact with different primary electron energies. We identify in the energy spectra, features that can be directly related to the underlying band structure. This, in turn, proves an important assumption in the theoretical description of the pair-emission process, namely that an effective single-particle picture for the electronic structure is an adequate description. With this observation, it is possible to identify the orbital character of the participating valence state. The relative pair-emission intensity from the surface state and 3*d* states is observed to vary dramatically with the primary energy. We observe particular conditions where the contribution from the Shockley surface state is strong. We propose a simplified model to explain this observation.

DOI: 10.1103/PhysRevB.84.125106 PACS number(s): 73.20.At, 79.60.−i

I. INTRODUCTION

The electron-electron interaction manifests itself in the emergence of many-body effects; we may name ferromagnetism and superconductivity as examples.[1] A key concept of solid state theory is the formation of the so-called exchange-correlation hole. This means that each electron is surrounded by a reduced electronic charge due to the Pauli principle, which prohibits two parallel spins to be at the same location, while the Coulomb interaction makes it energetically unfavorable for two electrons to be in close proximity, independent of the relative spin orientation. The concept of the exchange-correlation (xc) hole was introduced by Wigner and Seitz[2] and Slater.[3] In his seminal paper, Slater suggests that the xc hole does not depend strongly on the orbital character.[3] Experimentally we have demonstrated that the xc hole can be observed by studying the electron-pair emission from surfaces.[4–7] We found that the angular distribution exhibits a region of reduced intensity, which we termed depletion zone. In order to address Slater's suggestion, it would be highly desirable to find experimental conditions where the pair emission from a particular orbital state is enhanced compared to states with different orbital quantum numbers. Recent advances in the instrumentation make it possible to obtain pair-emission spectra covering an increased range of primary energies. With this capability, we aim to explore the validity of an important assumption of the theoretical description for the $(e,2e)$ process, which is an effective single electron description of the electronic properties of the sample.[8–11] The initial state is given by a Bloch state and an incoming primary electron described by a low-energy electron (LEED) state. The Bloch state is described by an effective single-particle (or quasiparticle) band structure that displays a strongly peaked density of states (DOS). The outgoing electrons defining the final state are time-reversed LEED states, which are not expected to display a strongly peaked structure as a function of the energy. Within this picture, the energy distribution of the emitted pairs should display peaks at the position of a high DOS of the Bloch state. However, one may wonder whether the effective single-electron description is adequate. Photoemission studies have revealed that many-body effects should be included;[12–14] in the case of transition metals, they result in a significant broadening of the quasiparticle peaks. The emergence of satellites in the photoemission spectrum of Ni is clearly beyond a quasiparticle picture.[15–18] Deviations from this are also known from the seemingly simple metal Cu.[19] Keeping in mind that pair-emission spectroscopy is particularly sensitive to the electron-electron interaction,[8–11] it is by no means clear whether an effective single-particle picture is adequate. If on the other hand, this description of the valence state is appropriate, the orbital character of the valence state can be identified, and it would be of interest to find conditions where the emission is dominated by a particular valence state. In order to test the conjecture, we selected a Cu(111) surface, which has a well-known electronic structure on the basis of theory and experiments.[20–25] Besides a bulk band structure characterized by rather flat 3*d* levels and strongly dispersing *sp* states, this surface possesses a surface state localized near the Fermi level E_F and confined to a small region around the center of the surface Brillouin zone. Near the bottom of the *d* band exists also a second surface state.[25] In this work, we report on $(e,2e)$ spectra from a Cu(111) surface for different values of the primary energy E_P and experimental geometries. We demonstrate that it is possible to identify electronic states in the energy spectra confirming an important point of the theoretical description. Furthermore, we observe that the intensity from the Shockley surface state can be significantly higher than from *d* states despite the fact that the number of occupied states in the *d* band is much higher. We suggest a simple model for predicting favorable conditions, which is based on a kinematical picture of electron-pair diffraction.

II. EXPERIMENTAL DETAILS

A sketch of the overall layout of the experiment is shown in Fig. 1.[26,27] It consists of two hemispherical electron-energy analyzers with a mean radius of 200 mm equipped with wide-angle transfer lenses and position-sensitive detectors.[28] The requirements of coincidence experiments required significant modifications. The standard detection scheme consists of a channel plate and a phosphorous screen imaged by a charge-coupled device (CCD) camera. This scheme does not allow for single-electron detection of the impact position. Consequently, we replaced the detectors by the installation of microchannel plates (MCP) with a 40-mm diameter active area

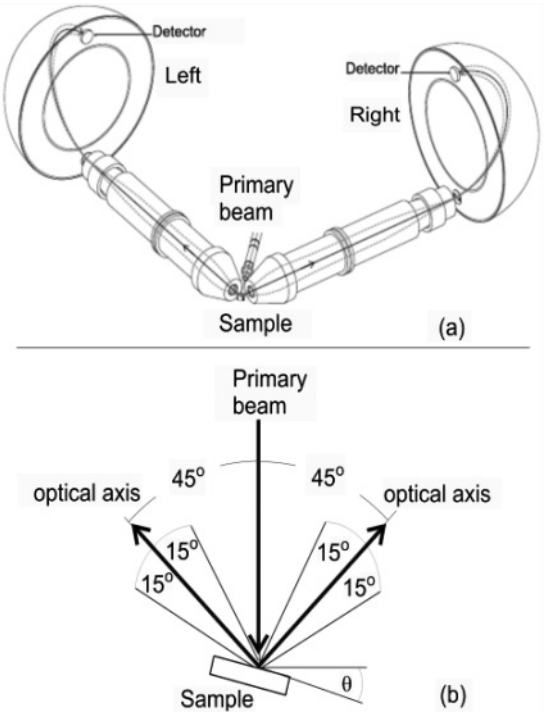

FIG. 1. (a) Experimental geometry of the coincidence electron spectrometer. It shows two hemispherical electron-energy analyzers that define a scattering plane and the [$\bar{2}$11] direction of the Cu(111) surface lies within the scattering plane. The excitation source is focused onto a Cu(111) surface. (b) The electron optical axis of the setup where the transfer lenses are symmetrically positioned in the same plane as the primary beam such that the outgoing electrons were detected at $\pm 45^\circ$ with respect to the surface normal (in the case of $\theta = 0^\circ$). The angular acceptance range of $\pm 15^\circ$ with respect to mean take-off angle is also shown.

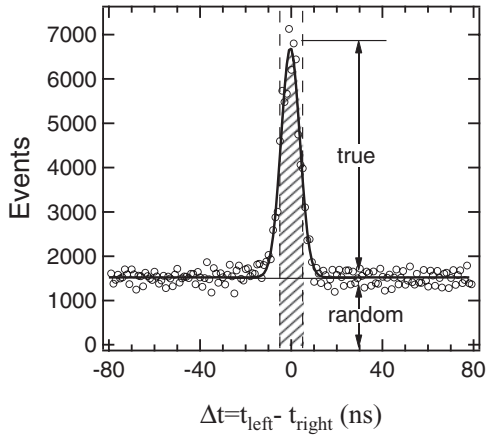

FIG. 2. Intensity vs arrival time differences (Δt) for all detected electron pairs. At $\Delta t = 0$ ns, the area beneath the observed peak and the constant intensity level corresponds to true coincidences. In the time difference histogram, the background is due to random coincidences, which is uniformly distributed over the time window. The thick solid line is shown to guide the eye. The dashed vertical lines at $\Delta t = \pm 5$ indicate the time window, which we used to generate the two-dimensional energy distribution.

and a resistive anode.[29] Coincidence experiments, in general, suffer from low count rates hence it is desirable to measure a large energy window in parallel. A typical value would be the band width of metals of the order 10 eV. The energy interval the spectrometers can cover in parallel is 10% of the pass energy. This means a pass energy of 100 eV is appropriate. At the same time we need to detect kinetic energies as low as a few eV. To fulfill this requirement, it was necessary to simulate the electron trajectories in the lens by commercial software.[30] Besides a high transmission, it has to be ensured that the temporal dispersion is minimized in order to reduce the contribution from unwanted events.[31] In contrast to the usual operation of electron spectrometers, we do not scan the energy but keep all electron-optical components constant for a given primary energy. We employ a four-way coincidence circuit in which the channel plate signals originating from the two spectrometers have to be within a time interval of 150 ns while the electronics of the resistive anodes indicate a successful impact position determination. The latter is required to determine the kinetic energy E_{left} and E_{right} of the coincident electrons. If a valid event is registered, the arrival times (t_{left} and t_{right}) with respect to the coincidence trigger can be determined. It is straightforward to determine the arrival time difference $\Delta t = t_{\text{left}} - t_{\text{right}}$ distribution and we show a typical histogram in Fig. 2. This distribution consists of an intensity peak centered at $\Delta t = 0$ residing on a constant background. If the detected electron pair stems from a single-step process ejecting two electrons with similar energy, then both electrons have to reach their respective detectors at the same time within the time resolution of the instrument. The time resolution can be directly determined from the peak in the curve, which has a width of $\approx$10 ns. The very existence of a peak in Fig. 2 is evidence of true coincidences. However, a fundamental problem is the existence of so-called random coincidences, which are due to the fact that two primary electrons may hit the target within the time resolution of the experiment and cause the emission of two uncorrelated electrons. This manifests itself by the constant intensity for all time difference Δt values. Our time resolution is 10 ns while we allow detection even for arrival time differences Δt up to 150 ns. It is clear that at those large Δt values only random coincidences are possible. The advantage of operating with a coincidence condition less stringent than the temporal dispersion is twofold. On the one hand, one can easily observe the ratio of true versus random coincidences. Due to the fact that for random coincidences, no time relation between the detected electrons exists, it is safe to assume that the constant intensity outside the peak region will also extend into the peak region. In this case, the number of true coincidences is given by the area between the peak and the constant background. Random coincidences determined for the same time interval are given by the area between the constant intensity and the zero line. For the experiments reported in this work, the ratio true/random was approximately 1.6. The singles count rates were about 3000 counts per second while the coincidence count rate was 2–3 counts per second. For the analysis of our energy spectra (to be shown below), we selected only those coincidences which are in the window $\Delta t = \pm 5$ ns, see vertical dashed lines in Fig. 2. This time window has been chosen after a detailed statistical analysis of 2D energy distributions, which yielded the best compromise between the total number of counts and

ratio of true/random. Another advantage of operating with the large coincidence window comes from the fact that it allows to determine the energy distribution of random coincidences without any contribution from true coincidences. Although it is strictly not possible to separate the random from the true coincidences, it is possible to separate the aggregate effect of random coincidences. In this scheme, one takes the total spectrum obtained by selection of a time window, e.g., the dashed vertical lines in Fig. 2. From this contribution, we subtract the random contribution obtained outside the peak region but with a time window of identical width. In this sense, we can obtain what we call the net spectrum. The electrostatic design of our setup allows us to make the measurements with constant energy resolution, which is independent of the measured kinetic energies. This is a clear advantage over the time-of-flight approach employed previously where the energy resolution degrades rapidly if the kinetic energy of the electrons increases.[32,33] This prohibits experiments beyond a primary energy of, say, 35 eV. The best compromise between energy resolution and count rate was attained by operation at 100 eV pass energy and 1 mm slit width. The overall energy resolution of the setup is ≈0.7 eV as judged from the sum energy spectra. The contribution of the electron gun was 0.3 eV due to the use of a BaO cathode.[34] The effect of the earth magnetic field has been reduced by using external Helmholtz coils and a mu-metal chamber. The base pressure of the chamber was $\approx 4\times 10^{-11}$ mbar. The Cu(111) surface was cleaned following standard procedures, which involve sputtering by 2 keV Ar^+ ions and subsequent annealing at approximately 875 K. The sample was at room temperature during the measurements. In the normal incidence geometry, the detectors were placed in a symmetric position at ±45° with respect to the electron beam axis [$\theta = 0°$ case in Fig. 1(b)] where the angular acceptance is ±15° for both the detectors within the scattering plane. Both detectors define a scattering plane in which the $[\bar{2}11]$ direction of the Cu(111) surface lies. We also performed experiments with non-normal incidence, which is described by a polar angle $\theta \neq 0$.

III. KINEMATICS AND GENERAL CONSIDERATIONS

For a $(e,2e)$ experiment on a crystalline surface momentum (within the surface plane) and energy conservation has to hold. As far as momentum conservation is concerned, we can write

$$k_{||}^{p} + k_{||}^{v} = k_{||}^{\text{left}} + k_{||}^{\text{right}} + g = k_{||}^{\text{sum}} + g, \tag{1}$$

where $k_{||}^{p}$ and $k_{||}^{v}$ are the contribution from the primary electron beam and valence-band electron, respectively. The momenta of the two outgoing electrons are given by $k_{||}^{\text{left}}$ and $k_{||}^{\text{right}}$, while g is a reciprocal lattice vector within the scattering plane. It is important to recognize that the emitted electrons form a single entity, which is characterized by a sum momentum: $k_{||}^{\text{sum}} = k_{||}^{\text{left}} + k_{||}^{\text{right}}$ and sum energy $E_{\text{sum}} = E_{\text{left}} + E_{\text{right}}$. We rewrite Eq. (1) to yield

$$k_{||}^{v} = k_{||}^{\text{sum}} - k_{||}^{p} + g. \tag{2}$$

We learn the important fact that the momentum of the valence electron can be inferred from the emitted pair. Low kinetic energies allow to set $g = 0$. This is very similar to a LEED experiment, where first-order diffraction beams are only present if a minimum energy is exceeded. Energy conservation within a $(e,2e)$ process can be formulated as

$$E_P + E_B^v = E_{\text{left}} + E_{\text{right}} + \phi = E_{\text{sum}} + \phi. \tag{3}$$

The primary electron energy is given by E_P, while the binding energy of the valence electron is determined by E_B^v. The kinetic energies of the emitted electrons are E_{left} and E_{right}, respectively. Since we effectively remove one electron from the sample, we have to take into account the work function ϕ of the sample, which in the case of a Cu(111) surface is ≈5 eV. The outgoing electron pair is characterized by the sum energy $E_{\text{sum}} = E_{\text{left}} + E_{\text{right}}$. We rearrange Eq. (3) and obtain

$$E_B^v = E_{\text{sum}} + \phi - E_P. \tag{4}$$

This means the binding energy of the valence electron is defined essentially by the sum energy. Hence, the position of the valence electron within the electronic band structure is known. At this point one has to specify what exactly is meant by electronic band structure. Within single-electron spectroscopy, say photoemission, an effective single-electron picture has proven to be sufficient.[37] However, in order to find agreement with experimental spectra, corrections to the theoretical band structure had to be made. The particular case of a Cu(111) surface was discussed in this context.[19] The motivation to perform $(e,2e)$ experiments and to describe the spectra theoretically stems from the fact that these studies are aimed to expand the description beyond an effective single-particle picture. The very existence of a correlated electron can not be formulated within an effective single-particle picture. The minimum step beyond this is to define two-particle wave functions for the $(e,2e)$ process. The current state-of-the art theory uses as the initial state a primary electron described as a LEED state and a Bloch state from a single-particle band structure calculation. The outgoing electron pair consists of two time-reversed LEED states coupled by a so-called "correlation factor".[8–11,38] Then the interaction between the initial and final state is mediated by a screened Coulomb interaction within the solid and the bare Coulomb interaction in the vacuum region. This framework has shown to be a satisfactory description of the experimental evidence in particular with respect to the angular distribution of the coincidence intensity. A key assumption in this theory is the use of an effective single-particle description for the valence state.[8–11,38] A consequence is that energy distributions can only have intensity where the occupied density of states (DOS) is nonvanishing. Experimentally it has become possible to obtain energy spectra with a sufficient energy resolution and spectral purity to investigate this aspect and check its validity.

We would like to recall some basics of the electronic band structure of the Cu(111) surface. In Fig. 3, we display the density of states of the surface layer at the Fermi level E_F as a function of the in-plane momentum.[35,36] High intensity is found near the zone boundary where the strongly dispersing s,p states cross the Fermi level. Near the center of the Brillouin zone, we see a circular region. In the bulk, there are no states within this region, however, at the surface a well-known state exists (Shockley surface state).[20–25,35,37] On the theoretical momentum distribution we have indicated with horizontal lines the momentum range our setup covers for

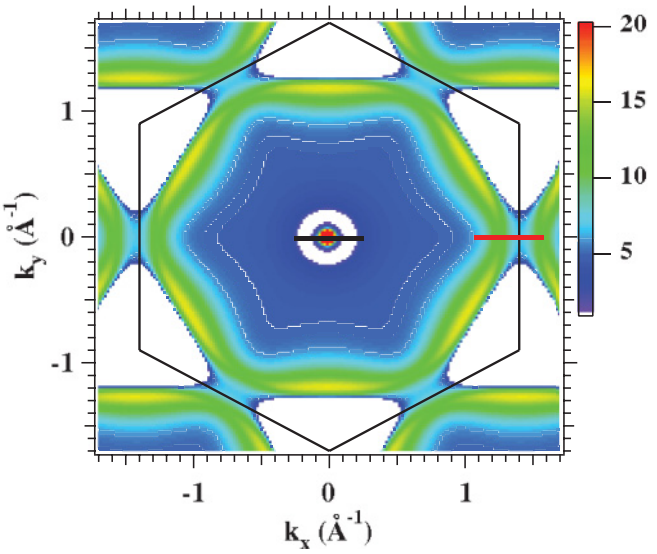

FIG. 3. (Color) Two-dimensional momentum distribution of the DOS of the first layer at $E_F - 0.4$ eV for a Cu(111) surface.[35,36] The black and red bars indicate the momentum range covered by our setup for different experimental geometries. The circle represents the energy gap at $\bar{\Gamma}$ point.

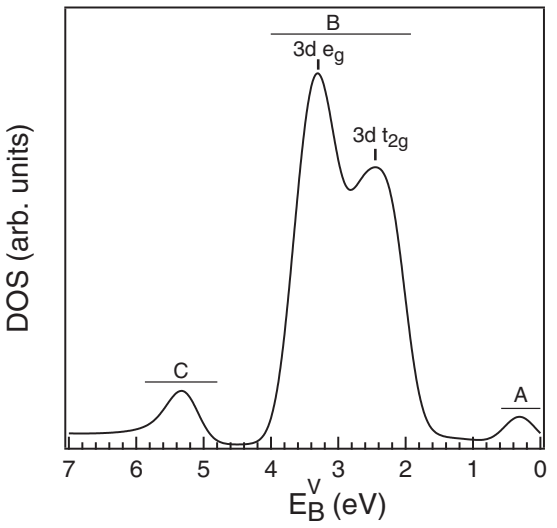

FIG. 4. The calculated density of states (DOS) for the Cu(111) surface is shown integrated over the angular acceptance and convoluted with a 0.5-eV-wide Gaussian.[35,36] The momentum integration corresponds to the black line of Fig. 3. For future reference, we label spectral regions with A, B, and C.

typical primary energies and the two geometries employed. The length follows immediately from Eq. (2) if we recall that we integrate over the full angular acceptance of both spectrometers. The black line concerns normal incidence excitation, although the width in momentum range is rather large with ± 0.5 Å^{-1}, it is nevertheless sufficiently small to probe the Shockley surface state within the bulk gap without integrating over the s,p electrons for which $|k_{||}^v| \geqslant 0.4$ Å^{-1}. The "red" line refers to the geometry where the polar angle $\theta = 15^\circ$. In this case, we are sensitive to states near the zone boundary where the s,p states are crossing the Fermi level.

In Fig. 4, we present the calculated binding energy spectrum of the occupied valence states.[35,36] For this, we have integrated the theoretical band structure over the experimental momentum window centered at the Brillouin center (black line), see Fig. 3. In order to aid comparison with experimental spectra, we convoluted with a Gaussian of 0.5 eV width representing the experimental resolution. The (e,2e) experiments are very surface sensitive and we averaged the layer-resolved DOS by taking into account appropriate weighting factors. The result is shown in Fig. 4 and three prominent features can be recognized. These we label with A, B, and C. Peak A resides near the Fermi level and is identified as the Shockley surface state. Region B consists of a range of various d states of which only two prominent distributions can be observed after convolution. Finally, region C consists of the bottom of the d band and a second surface state.[25] Therefore we expect to observe in the sum energy spectra coincidences only at those energies that are due to the regions A, B, and C.

IV. RESULTS

A. Normal incidence excitation

The 2D energy distribution of correlated electron pairs for excitation with a primary beam of $E_P = 29.2$ eV is shown in Fig. 5. The spectrum contains those coincidence events for which the arrival time differences fulfill $|\Delta t| < 5$ ns. This amounts to the shaded peak region displayed in the Δt histogram, see Fig. 2. The axes are the individual energies E_{left} and E_{right}, respectively. In panel (a), we plot the spectrum including true and random coincidences. Energy conservation demands that the sum energy has an upper bound $E_{\text{sum}}^{\text{max}}$, which can be written as

$$E_{\text{sum}}^{\text{max}} = E_P - \phi. \tag{5}$$

In this case, the emission of a valence electron from the Fermi level takes place. A constant sum energy can be visualized in the 2D energy plot as a diagonal line, therefore we have indicated the line $E_{\text{sum}}^{\text{max}}$ in panel (a) as a black dotted diagonal line. We can clearly observe that the coincidence intensity starts to rise once E_{sum} falls below the diagonal line. The weak intensity above this line must be due to random coincidences, because in this case, twice the primary energy is available and Eq. (5) is not valid.

As explained earlier, it is possible to remove approximately the aggregate effect of the random coincidences by determining the 2D energy spectrum of random coincidences. The corrected spectrum containing only the net coincidences is displayed in Fig. 5(b). The main difference between Figs. 5(a) and 5(b) is the removal of intensity above the $E_{\text{sum}}^{\text{max}}$ line labeled with A in panel (b). Two red lines of constant sum energy have been added to panel (b), which are labeled B and C, respectively. We note enhanced intensity along these lines which shows more contrast in panel (b). It is useful to present the coincidence data in a E_{sum} spectrum. The symmetry of the experiment suggests to set $E_{\text{left}} = E_{\text{right}}$. However, in order to obtain sufficient statistics, we lower the constraint and allow all events, which fulfill $E_{\text{left}} = E_{\text{right}} \pm 3$ eV. This constraint is visualized by the pair of dash-dotted parallel lines in panel (b) and will be imposed on all E_{sum} spectra to be

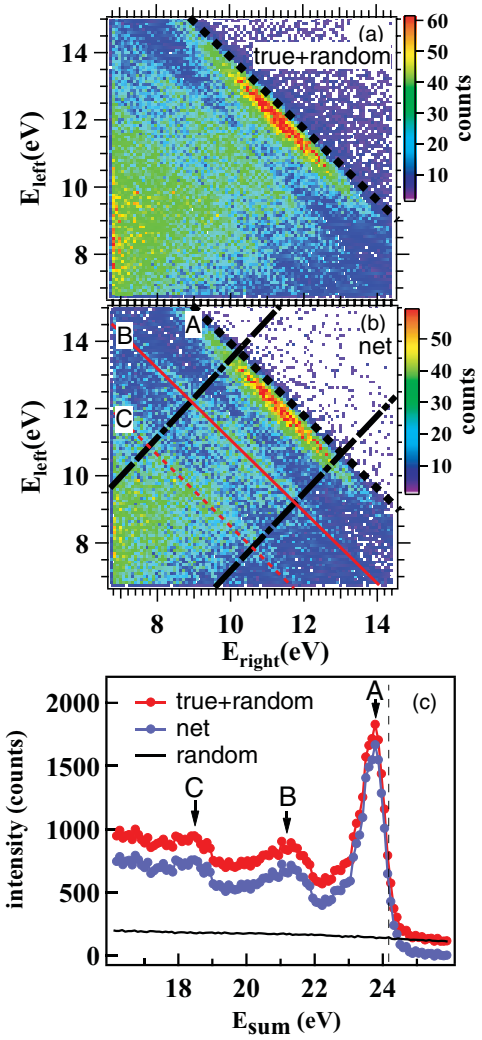

FIG. 5. (Color) 2D energy plots for $E_P = 29.2$ eV (a) raw data and (b) after removal of the random contribution. The dashed black diagonal line marks the onset of pair emission from E_F, which occurs for $E_{sum} = 24.2$ eV. The bars on the right side define the color codes for the intensity given in counts. Black dashed-dotted lines in (b) show the region for which $E_{left} = E_{right} \pm 3$ eV. (c) The E_{sum} spectra are computed by integrating the intensity for $E_{left} = E_{right} \pm 3$ eV. The regions marked by A, B (red solid line), and C (red dashed line) in (b) correspond to the respective features in the E_{sum} spectra in (c).

shown in this work. The result of this procedure is plotted in Fig. 5(c). The intensity of true+random events that fulfilled the condition $|\Delta t| \leqslant 5$ ns is given by the red curve, while the blue curve contains the net spectrum. The random spectrum alone is shown by the black line, which is essentially featureless. This demonstrates that the spectral features of true+random reflect the structures in the net spectrum. The described way of the removal of random coincidences has been established in electron-pair emission spectroscopy in the past even in those instances where the random distribution is not featureless.[39,40] In the following, we present E_{sum} spectra that are corrected in this manner.

Let us focus on the actual net (blue) E_{sum} spectrum. In this curve, we can easily recognize three peaks which are labeled A, B, and C; the position of E_{sum}^{max} is given by the dashed vertical line at 24.2 eV. These peaks are the counterpart of the peaks plotted in Fig. 4. They occur at the correct energy position and the width can be explained by the instrumental resolution. This point is of great importance since it shows that the assumption of a single-particle band structure in the current theoretical description is valid at least for Cu(111). Experimentally, we can not determine the individual contributions of bulk and surface state of peak C. It should not come as a surprise that the relative intensities are different from the DOS distribution, because the transition probabilities from different valence states are not constant. Surprising though is the very large contribution from peak A, which comes from the Shockley surface state; we come back to this point later.

We continue and discuss the primary energy dependence of the E_{sum} spectra. We compare in Fig. 6 two more experimental results together with the 2D energy distribution shown already in Fig. 5(b). As before, the position of E_{sum}^{max} is given by the dashed black line. In panel (a), we show the data for $E_P = 19.2$ eV and it is apparent that compared to the plot of panel (b), the spectrum is dominated by the intensity near E_{sum}^{max}, only two very faint intensity regions for lower-sum energies can be seen. We note that the high intensity occurs only if both electrons have similar energies. In Fig. 6(c), we present the result for the highest E_P value studied in this work. Here, the spectrum is dominated by a band of intensity, which is roughly 3 eV below E_{max}^{sum}; these are due to the $3d$ states associated with the peak B, see Fig. 4. Obviously, the spectral shape does depend on the primary energy. However, the intensity peaks are still at positions determined by the single-particle band structure shown in Fig. 4. A more concise view of the energy dependence on the pair emission can be obtained by comparing E_{sum} spectra, which we present in Fig. 7. As a matter of fact, it is more appropriate to plot the intensity as a function of $E_{sum} - E_{sum}^{max}$. This has the advantage that emission from the same valence state occurs at the same energy position. The vertical dashed line at $E_{sum} - E_{sum}^{max} = 0$ indicates emission from E_F. For $E_P = 19.2$ eV, the main contribution in the coincidence intensity stems from states near E_F, while the d states at about 3 eV below E_F hardly contribute. As we increase E_P, the relative intensity of the d states increase with respect to the Shockley surface state. Finally, for $E_P = 65.2$ eV, the Shockley surface state intensity almost disappears while the main contribution comes from d states. The dependence on the primary energy is not surprising, a detailed understanding would involve a thorough theoretical account. Nevertheless, we achieved the goal to identify conditions where the emission is dominated by states of a particular orbital character. The high intensity from the Shockley state deserves some more comments. Inspection of Fig. 6(a) shows that the high intensity near E_{sum}^{max} occurs for almost equal energies E_{left} and E_{right}. Equal energies and equal but opposite emission directions will ensure that $k_{sum} = 0$, which is fulfilled for the surface state. A more appropriate presentation is to compute so-called sharing curves. This is the coincidence intensity as a function of $E_{left} - E_{right}$ for a fixed E_{sum}. Specifically, we integrate over E_{sum} values from E_{sum}^{max} to $E_{sum}^{max} - 0.7$ eV, which includes energetically the Shockley surface state. The result for different primary energies is shown in Fig. 8. For $E_P = 19.2$ eV, we see clearly that the main

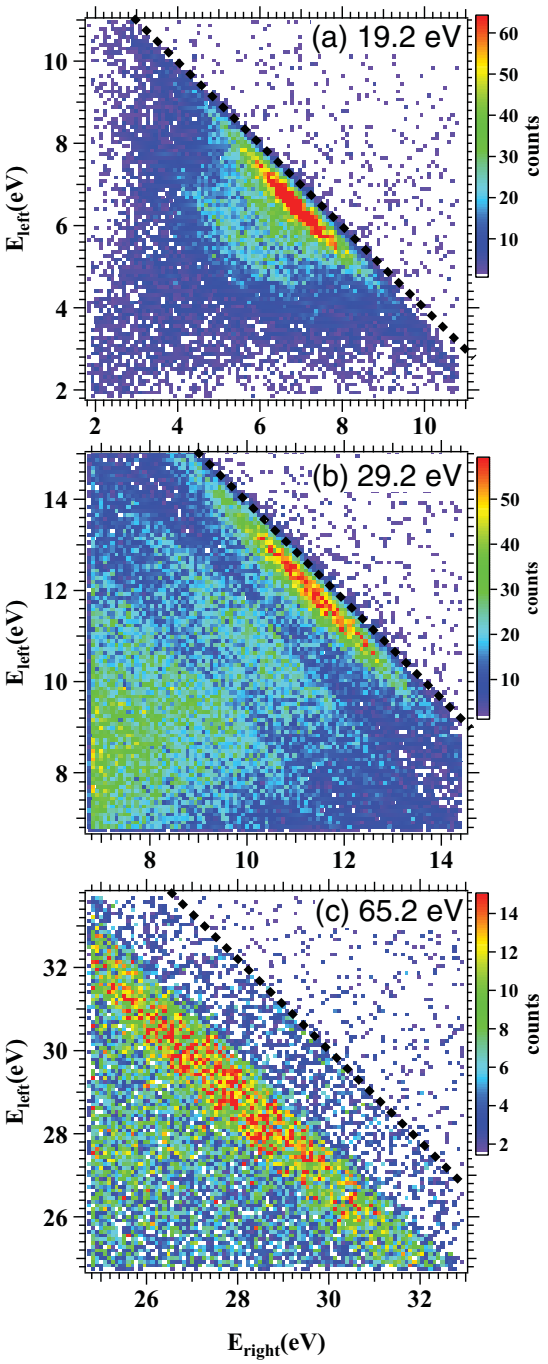

FIG. 6. (Color) 2D energy spectra obtained from Cu(111) excited with different primary energy $E_P = 19.2, 29.2$, and 65.2 eV in normal incidence. The dashed diagonal lines indicate the energetic position of $E_{\text{sum}}^{\text{max}}$.

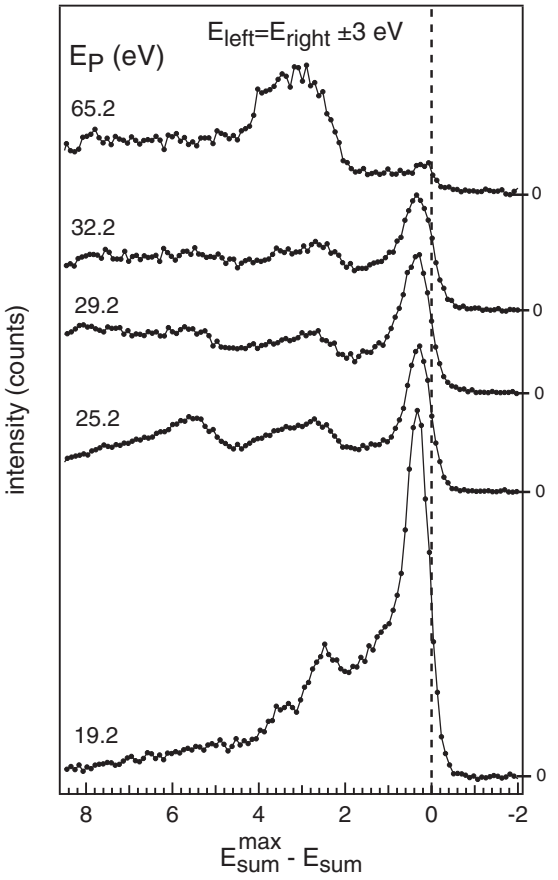

FIG. 7. Sum energy spectra as a function of primary electron energy computed for the $E_{\text{left}} = E_{\text{right}} \pm 3$ eV condition. The vertical dashed line is the energy position of the highest possible sum energy, which is equivalent to the zero of two-electron binding energy. The spectra are staggered along the vertical axis for clarity of presentation.

intensity occurs for $|E_{\text{left}} - E_{\text{right}}| < 2$ eV. Upon increasing E_P, the peak decreases until it disappears at $E_P = 35.2$ eV, see Fig. 8. For this primary energy, the intensity is essentially constant. Upon increasing E_P to a value of 45.2 eV, the peak in the sharing curve reemerges. Upon further increase of E_P, the peak disappears and does not occur within the primary energy window covered in this work. We can make two statements regarding the emission from the surface state. First, at certain primary energies, the emission from this state makes a large contribution to the overall intensity. Second, the emitted pairs tend to have equal energies for certain primary energies. This latter point is surprising because we recall that the surface state resides in a momentum range of ± 0.2 Å^{-1}. If we take into account the finite angular acceptance, a purely kinematical consideration will reveal that the emission from the Shockley surface state should occur for all energy differences within the energy window of the instrument. In order to fully trace down the origin of these observations, a dedicated $(e,2e)$ calculation needs to be performed, which is outside the scope of this work. The theoretical description invokes a multiple scattering approach.[9] Therefore we aim to use the simplest approximation of this framework, which is a kinematical description. An electron pair constitutes a single entity for which diffraction effects similar to LEED are expected. As a matter of fact it has been demonstrated experimentally that electron-pair diffraction occurs at surfaces.[41,42] This can be easily understood by recalling Eq. (2), which describes that the in-plane momentum of the pair is conserved modulo a reciprocal lattice vector. This is a diffraction condition. It is also established that LEED is sensitive to the perpendicular lattice constant. Measuring the LEED intensity of the diffraction spots as a function on the primary energy (so-called LEED I-V curves) is a tool to determine the layer separation of the first, say, five atomic layers. For this, it is required to employ

a multiple scattering theory. On the other hand, it is known that a simple kinematical description of the (0,0) beam gives a reasonable estimate of the layer-averaged perpendicular lattice constant. In this picture, the intensity maxima of the (0,0) *I-V* curve are due to a constructive interference condition. It is our aim to extend this model to electron pairs. For LEED, the primary energy E_P^{00} at normal incidence that results in a Bragg peak is given by the equation:[43]

$$E_P^{00} = \frac{n^2h^2}{8md^2} - V_0, \quad n = 1,2,\ldots. \tag{6}$$

The inner potential V_0 is for Cu $\approx$10 eV. The electron mass and Planck constant are given by m and h, respectively. The layer separation is determined by d. The prediction of this model is in fair agreement with the experimental observation.[44,45] The picture on which the above equation is based determines the wavelength λ inside the crystal for which the condition $2d = n\lambda$ must hold. Obviously, choosing $n = \frac{1}{2}, \frac{3}{2}, \ldots$ leads to destructive interference. It is now straightforward to formulate a constructive interference condition for pairs. For an electron pair to have the same wavelength as a single electron, the energy inside the crystal has to be half of the value for one electron. The emission direction with respect to the normal also enters the description, which in our experiment is 45°, see Fig. 1. In order to determine the pair energy inside the crystal, we have to consider the inner potential of a pair. The simplest approximation is to take twice the value for a single electron. Further, we have to consider the work function and binding energy of the valence electron. For convenience, we can group some of the terms to yield the expression for E_p^{00} as in Eq. (6). This finally leads to the following equation for the primary energy E_P for which diffraction of pairs along the normal direction occurs:

$$E_P^{\text{pairs}} = \tfrac{1}{2}E_P^{00} - \tfrac{3}{2}V_0 + E_B + \phi. \tag{7}$$

Because the term $\frac{1}{2}E_P^{00}$ includes already a term $\frac{1}{2}V_0$, we find in Eq. (7) the term $\frac{3}{2}V_0$ rather than $2V_0$. The counterpart of an elastically reflected primary electron is an electron pair whose energy is determined by E_p, binding energy, and work function but no further inelastic processes. For the Shockley state, $E_B = 0$ eV and one expects the first two Bragg maximuma for $E_P = 24$ and 54 eV, while at $E_P = 38$ eV destructive interference occurs. Although this energy sequence is numerically not in agreement with experiment it does explain the formation of a peak in the sharing curve, which disappears and reemerges as a function of primary energy. Further peaks are expected for higher primary energies, but these predicted peaks are outside the primary energy window of the current study. Undoubtedly, the kinematical description is rather crude, but we would like to point out that state-of-the art calculations of the (*e*,2*e*) intensity invoke a multiple scattering approach.[9] This means that many different scattering paths exist that need to be included. We suggest that the leading contribution as far as the Shockley surface state is concerned stems from the diffraction of pairs along the surface normal.

The operator describing the transition in a (*e*,2*e*) process is a screened Coulomb potential in contrast to the dipole operator in photoemission. Nevertheless, further support for our kinematical model comes from photoemission studies on Cu(111) and Ag(111) surfaces. There, it was noted that for certain photon energies enhanced intensity from surface states was observed. This resonance was explained within a model in which a key ingredient was constructive interference along the surface normal.[25,46,47]

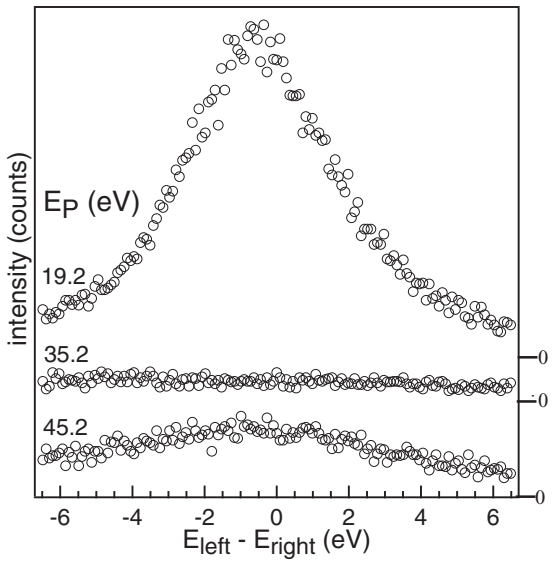

FIG. 8. Sharing curves obtained for different primary energies E_P and the constraint $|E_{\text{sum}} - E_{\text{sum}}^{\text{max}}| \leqslant 0.7$ eV. This selection ensures that the Shockley surface state is in the energy field of view. Due to kinematical reasons emission from this state has to occur for $E_{\text{left}} - E_{\text{right}} \approx 0$. The spectra are staggered along the vertical axis for clarity of presentation.

B. Off-normal incidence excitation

In normal incidence, we have established that the E_{sum} energy spectra show peaks directly related to the valence band structure. It is appealing to investigate whether we can also follow the dispersion of the band structure. Therefore we changed the polar angle to 15° and probe the Brillouin zone near the zone boundary, see Fig. 3. In this case, the Shockley surface state can not make a contribution. In Fig. 9, we compare the E_{sum} spectra obtained with $\theta = 0°$ and 15° together with the theoretical DOS curves. The latter have been obtained via the same momentum integration, energy convolution, and weighted layer averaging as discussed in the context of Fig. 4. The experimental data are plotted as a function of $E_{\text{max}} - E_{\text{max}}^{\text{sum}}$, which allows direct comparison with the DOS spectrum. Let us discuss the peak region C first. In the experiment, we observe one peak, which is shifted by 0.5 eV toward higher energies, which shows a weak shoulder on the high-energy side. The DOS spectrum reveals also a small shift of 0.2 eV while a second peak appears at the high energy side. The main difference to the experiment is that the high-energy part has a higher spectral weight compared to the experiment.

Comparison of the experimental spectra for region B reveals some movement but the line shape variation suggests more a reduction of intensity at the low binding energy side of peak B.

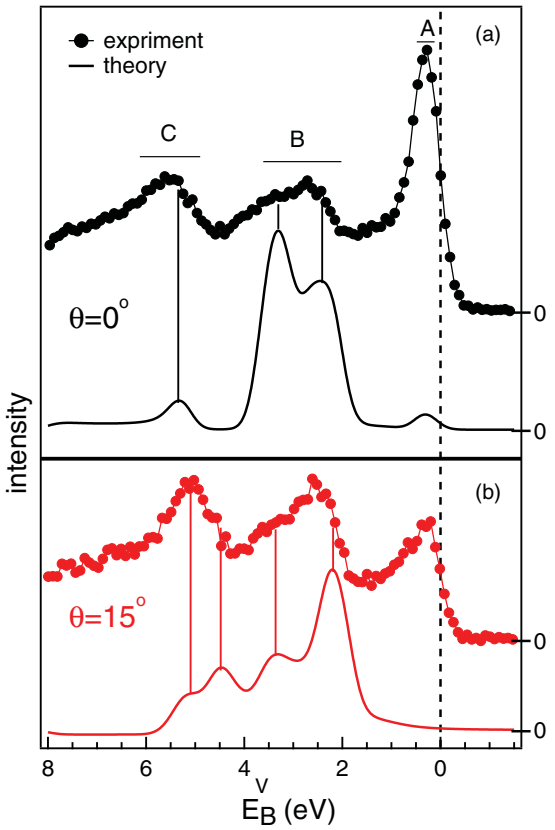

FIG. 9. (Color) We show the sum energy spectra together with the DOS. The experimental data are given by the solid dots, whereas the DOS is given by the continuous curve. In panel (a) we compare the result for $\theta = 0^\circ$, while in (b) the result for $\theta = 15^\circ$ is shown. The primary energy is $E_P = 29.2$ eV. The spectra are shifted along the vertical axis for clarity of presentation.

Such a notion is supported by the DOS spectrum since a peak at the high energy side of region B becomes stronger upon changing to $\theta = 15^\circ$.

The intensity of peak A with respect to the other components has reduced although it is still sizable. For $\theta = 0^\circ$, we have to expect a peak near E_F due to the Shockley surface state, for $\theta = 15^\circ$, we are probing a narrow region in momentum space where the sp bands cross E_F. This means that there is no peak in the DOS. However, the experiment shows clearly a peak. This means that there is a process that emphasizes the emission from states near E_F. With this in mind we extent the pair diffraction model to non-normal incidence. It turns out that the energies for which one has to expect constructive interference along the normal are given by

$$E_P^{\text{pairs}} = \frac{E_P^{00} - 3V_0}{2 - \sin^2\theta} + \phi. \tag{8}$$

For $\theta = 15^\circ$, we can numerically ignore the sin term in Eq. (8) and expect diffraction to occur at the same energies as for normal incidence. Therefore we attribute the strong intensity of peak A to be due to a diffraction condition for pairs, which is fulfilled for valence electrons near E_F. From the off-normal incidence experiments, we learn that we are able to follow the dispersion of the single-particle band structure. This further supports the notion that for a theoretical description of the (e,2e) process the use of such a band structure is warranted at least for Cu. We found that there is a peak in the experimental data near E_F that does not have a counterpart in the DOS. We suggest that a diffraction of pairs along the surface normal leads to the formation of this peak.

V. SUMMARY

We present a systematic pair-emission study from a Cu(111) surface with the emphasis on energy distributions. Improved instrumentation allowed us to obtain spectra of higher purity and we extended the measurements to higher primary energies than before. The experimental approach is particularly sensitive to the electron-electron correlation. We find that the energy spectra can be well described by an underlying effective single-electron picture. This was *a priori* not obvious, since many-body effects are known to cause a deviation from a quasiparticle picture. Our observation for the case of Cu proves an important assumption of the theoretical description of a (e,2e) process, namely, to describe the valence state of the solid via an effective single particle band structure. The emission from valence states of different orbital character can be clearly observed and the relative contribution can be selected by the primary energy. The Cu(111) surface is known to exhibit a surface state near the Fermi level. We observed that at low primary energies the intensity is dominated by the contribution from this state. We suggest a simple kinematic diffraction model for pairs to explain this feature.

ACKNOWLEDGMENT

We thank F. Giebels, H. Gollisch, and R. Feder for stimulating discussions and making available to us the data of the band structure calculations. C. Winkler is thanked for support during the experimental work. Funding from the DFG through SFB 762 is gratefully acknowledged.

*schumann@mpi-halle.de
†Present address: Department of Physics, La Trobe University, Melbourne, Australia

[1] P. Fulde, *Electron Correlations in Molecules and Solids*, Springer Series in Solid-State Sciences (Springer, 1991), Vol. 100.
[2] E. Wigner and F. Seitz, Phys. Rev. **43**, 804 (1933).
[3] J. C. Slater, Rev. Mod. Phys. **6**, 209 (1934).
[4] F. O. Schumann, J. Kirschner, and J. Berakdar, Phys. Rev. Lett. **95**, 117601 (2005).
[5] F. O. Schumann, C. Winkler, G. Kerherve, and J. Kirschner, Phys. Rev. B **73**, 041404(R) (2006).
[6] F. O. Schumann, C. Winkler, and J. Kirschner, Phys. Rev. Lett. **98**, 257604 (2007).
[7] F. O. Schumann, C. Winkler, and J. Kirschner, New J. Phys. **9**, 372 (2007).
[8] R. Feder, H. Gollisch, D. Meinert, T. Scheunemann, O. M. Artamonov, S. N. Samarin, and J. Kirschner, Phys. Rev. B **58**, 16418 (1998).

[9]H. Gollisch, X. Yi, T. Scheunemann, and R. Feder, J. Phys. Condens. Matter **11**, 9555 (1999).
[10]J. Berakdar, H. Gollisch, and R. Feder, Solid State Commun. **112**, 587 (1999).
[11]H. Gollisch, N. v. Schwartzenberg, and R. Feder, Phys. Rev. B **74**, 075407 (2006).
[12]S. Monastra, F. Manghi, C. A. Rozzi, C. Arcangeli, E. Wetli, H.-J. Neff, T. Greber, and J. Osterwalder, Phys. Rev. Lett. **88**, 236402 (2002).
[13]J. Sánchez-Barriga, J. Fink, V. Boni, I. Di Marco, J. Braun, J. Minár, A. Varykhalov, O. Rader, V. Bellini, F. Manghi, H. Ebert, M. I. Katsnelson, A. I. Lichtenstein, O. Eriksson, W. Eberhardt, and H. A. Dürr, Phys. Rev. Lett. **103**, 267203 (2009).
[14]J. Sánchez-Barriga, J. Minár, J. Braun, A. Varykhalov, V. Boni, I. Di Marco, O. Rader, V. Bellini, F. Manghi, H. Ebert, M. I. Katsnelson, A. I. Lichtenstein, O. Eriksson, W. Eberhardt, H. A. Dürr, and J. Fink, Phys. Rev. B **82**, 104414 (2010).
[15]R. Clauberg, W. Gudat, E. Kisker, E. Kuhlmann, and G. M. Rothberg, Phys. Rev. Lett. **47**, 1314 (1981).
[16]G. van der Laan, M. Surman, M. A. Hoyland, C. F. J. Flipse, B. T. Thole, Y. Seino, H. Ogasawara, and A. Kotani, Phys. Rev. B **46**, 9336 (1992).
[17]F. Manghi, V. Bellini, J. Osterwalder, T. J. Kreutz, P. Aebi, and C. Arcangeli, Phys. Rev. B **59**, R10409 (1999).
[18]G. van der Laan, J. Zaanen, G. A. Sawatzky, R. Karnatak, and J.-M. Esteva, Phys. Rev. B **33**, 4253 (1986).
[19]R. Courths, M. Lau, T. Scheunemann, H. Gollisch, and R. Feder, Phys. Rev. B **63**, 195110 (2001).
[20]P. O. Gartland and B. J. Slagsvold, Phys. Rev. B **12**, 4047 (1975).
[21]S. D. Kevan, Phys. Rev. Lett. **50**, 526 (1983).
[22]J. A. Knapp, F. J. Himpsel, and D. E. Eastman, Phys. Rev. B **19**, 4952 (1979).
[23]P. Heimann, J. Hermanson, H. Miosga, and H. Neddermeyer, Surf. Sci. **85**, 263 (1979).
[24]R. Courths and S. Hüfner, Phys. Rep. **112**, 53 (1984).
[25]S. G. Louie, P. Thiry, R. Pinchaux, Y. Petroff, D. Chandesris, and J. Lecante, Phys. Rev. Lett. **44**, 549 (1980).
[26]G. A. van Riessen, F. O. Schumann, M. Birke, C. Winkler, and J. Kirschner, J. Phys. Condens. Matter **20**, 442001 (2008).
[27]G. A. van Riessen, Z. Wei, R. S. Dhaka, C. Winkler, F. O. Schumann, and J. Kirschner, J. Phys. Condens. Matter **22**, 092201 (2010).
[28]N. Mårtensson, P. Baltzer, A. Brambilla, P. A. Brühwiler, J. O. Forsell, A. Nilsson, A. Stenborg, and B. Wannberg, J. Electron. Spectrosc. Relat. Phenom. **70**, 117 (1994).
[29]Quantar Technology Incorporated, Model 3300 SERIES MCP.
[30]SIMION sold by Scientific Instruments Services Inc.
[31]M. Völkel and W. Sandner, J. Phys. E **16**, 456 (1983).
[32]S. N. Samarin, O. M. Artamonov, D. K. Waterhouse, J. Kirschner, A. Morozov, and J. F. Williams, Rev. Sci. Instrum. **74**, 1274 (2003).
[33]J. Kirschner, G. Kerherve, and C. Winkler, Rev. Sci. Instrum. **79** (2008).
[34]Kimball Physics Model ELG-2.
[35]F. Giebels, H. Gollisch, and R. Feder, J. Phys. Condens. Matter **21**, 355002 (2009).
[36]The theoretical band structure data required to make these plots where supplied by F. Giebels, H. Gollisch, and R. Feder. Details of the approach can be found on www.flapw.de
[37]S. Hüfner, *Photoelectron Spectroscopy* (Springer, 2003).
[38]N. Fominykh, J. Henk, J. Berakdar, P. Bruno, H. Gollisch, and R. Feder, Solid State Commun. **113**, 665 (2000).
[39]G. A. Sawatzky, *Auger photoelectron coincidence spectroscopy*, in *Auger Electron Spectroscopy*, edited by C. L. Briant and R. P. Messmer (Academic Press, San Diego, 1988).
[40]E. Jensen, R. A. Bartynski, S. L. Hulbert, and E. Johnson, Rev. Sci. Instrum. **63**, 3013 (1992).
[41]J. Berakdar, S. N. Samarin, R. Herrmann, and J. Kirschner, Phys. Rev. Lett. **81**, 3535 (1998).
[42]S. Samarin, J. Berakdar, O. M. Artamonov, H. Schwabe, and J. Kirschner, Surf. Sci. **470**, 141 (2000).
[43]J. Pendry, *Low Energy Electron Diffraction* (Academic Press, London, New York, 1974).
[44]S. Andersson, I. Marklund, and J. Martinson, Surf. Sci. **12**, 269 (1968).
[45]S. A. Lindgren, L. Walldén, J. Rundgren, and P. Westrin, Phys. Rev. B **29**, 576 (1984).
[46]S. D. Kevan, N. G. Stoffel, and N. V. Smith, Phys. Rev. B **31**, 1788 (1985)
[47]T. C. Hsieh, P. John, T. Miller, and T.-C. Chiang, Phys. Rev. B **35**, 3728 (1987).